Transport properties of quantum dot arrays

Jianwei Cai and G. D. Mahan
Department of Physics, Pennsylvania State University, University Park, Pennsylvania 16802, USA
(Received 6 March 2008; revised manuscript received 17 June 2008; published 14 July 2008)

The model of crystalline arrays of quantum dots is studied with dynamical mean-field theory. Low-temperature transport coefficients are calculated. The material is found to be metallic with a large Seebeck coefficient, which has a good promise for thermoelectric applications.

DOI: 10.1103/PhysRevB.78.035115 PACS number(s): 72.15.Jf, 71.10.Fd

I. INTRODUCTION

Heavy-fermion systems have been shown to have promise for thermoelectric applications both experimentally[1] and theoretically.[1,2] The advantage of such materials lies in the high thermoelectric coefficient due to the Kondo effect. A similar Kondo effect is present and widely studied in the quantum dots.[3–8] Nanoengineering can build new materials with arrays of quantum dots[9–11] that may take advantage of their Kondo effect for high thermoelectric coefficient. Other properties of the materials, including conductivity and thermal conductivity, can be tailored to improve the overall performance. An example of such nanoengineered materials, crystalline arrays of quantum dots connected by conducting chains of linkers, is proposed in a previous paper.[12] A prototype of such material is under study in Yuan *et al.*[13] The possible advantages of this material include better electrical conductivity due to the linker atoms, lower thermal conductivity due to the heavy mass of quantum dots, and higher thermoelectric coefficient due to the Kondo effect. These possible properties make the material interesting for thermoelectric applications.

In our theoretical model, we treat every quantum dot as an Anderson impurity in the periodic Anderson model (PAM).[3–5] Electrons in these sites are strongly correlated due to the on-site Coulomb interaction. These sites are called correlated sites. In the linker sites between quantum dots, such Coulomb interaction is absent. So they are treated as sites in a simple tight-binding model. This theoretical model can be considered as an extension of the Hubbard model by adding to it non interacting linker sites. This extension makes our model very different from the Hubbard model. The exchange interaction between two neighboring correlated sites in the Hubbard model is replaced by superexchange in our model. This results in different magnetic properties for our model, which may be the topic for future study. Another obvious difference is the metal-insulator transition, which appears in both the Hubbard model and the PAM,[14] does not appear in our model as shown below. Our model shows improved conductivity and Seebeck coefficient. The difference between our model and PAM has been discussed in length in a previous paper.[12]

The model is studied in the infinite-dimensional cubic lattice with dynamical mean-field theory (DMFT). The DMFT becomes exact for such infinite-dimensional lattice model[15] and is widely used for lattice models with strong interactions.[15,16] For our study, the infinite-dimensional cubic lattice is divided into two sublattices, which can be constructed according to following rule: the nearest neighbors of any given site are assigned to the opposite lattice. The two-dimensional example is shown in Fig. 1. One sublattice is occupied by conducting linkers. The other sublattice is occupied by the correlated sites. The effective single-impurity Anderson model (SIAM) from the mapping of this lattice model is solved by Wilson's numerical renormalization group (NRG).[17] The advantage of this impurity solver lies in its accuracy for the low-energy properties,[18] which is essential for this study. The self-consistency calculation is done at zero temperature. Transport properties at finite temperature are interesting. At temperatures much lower than the Kondo temperature T_K, the spectral functions and self energies can be approximated by the corresponding zero-temperature results. With such approximations, we can discuss the transport properties for our model using Kubo formulas at low temperature. The details of the theory are given in the next section.

We work in the paramagnetic phase. The local spectral function, optical conductivity, and Seebeck coefficient are studied. This study highlights the possibility of quantum dot arrays for thermoelectric applications.

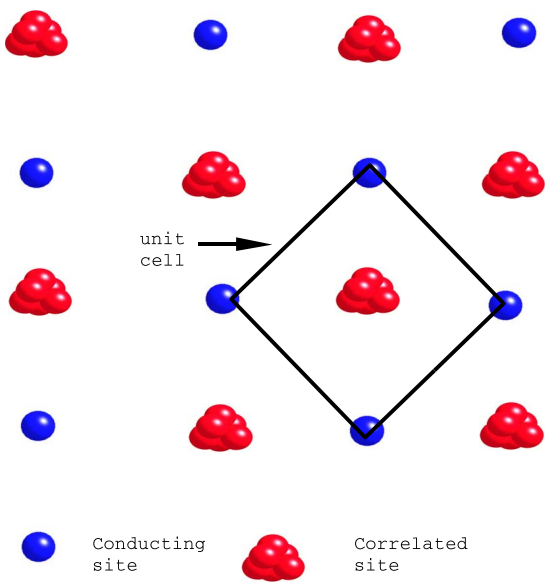

FIG. 1. (Color online) The two-dimensional version of the lattice considered in this study. The lattice we studied in the paper is the infinite-dimensional extension of it.

II. THEORY

The Hamiltonian for our model is given by

$$H = \sum_{i\sigma}\left[(\epsilon_f - \mu) f^\dagger_{i\sigma} f_{i\sigma} + \frac{U}{2} f^\dagger_{i\sigma} f_{i\sigma} f^\dagger_{i-\sigma} f_{i-\sigma}\right] + \sum_{i\sigma}(\epsilon_c - \mu) C^\dagger_{i\sigma} C_{i\sigma} + \sum_{i\sigma}\left(\sum_\delta t^* C^\dagger_{i+\delta\sigma} f_{i\sigma} + \text{H.c.}\right), \tag{1}$$

where $f_{i\sigma}(f^\dagger_{i\sigma})$ destroys (creates) an electron with spin σ and binding energy ϵ_f at correlated site i. μ is the chemical potential. U denotes the on-site Coulomb interaction. Similarly, $C_{i\sigma}(C^\dagger_{i\sigma})$ destroys (creates) an electron with spin σ and binding energy ϵ_c at linker site i. The last term describes the coupling between correlated sites and linker sites with matrix element t^*. For correlated site i, $i+\delta$ denotes the nearest linker sites. The two-dimensional version of this lattice is shown in Fig. 1. In order to have a nontrivial density of states, t^* must scale with $1/\sqrt{d}$,[15] where d is the dimension of the lattice. We set $t^* = t/\sqrt{2d}$ in this study. We assume the presence of some external bath that keeps the chemical-potential constant. This constant can be absorbed in ϵ_f and ϵ_c, and μ is dropped in the following formulas.

We take the distance between the nearest-neighbor sites to be the unit for distance. The nearest sites for site $i(x_1, x_2, x_3, \ldots)$ can be set as

$$i + \delta_{\pm 1} = (x_1, x_2, x_3, \ldots) + (\pm 1, 0, 0, \ldots),$$

$$i + \delta_{\pm 2} = (x_1, x_2, x_3, \ldots) + (0, \pm 1, 0, \ldots),$$

$$i + \delta_{\pm j} = (x_1, x_2, x_3, \ldots) + (0, 0, \ldots, \pm 1(j\text{th}), \ldots), \ldots .$$

The vectors between neighbors define all possible lattice vectors.

$$a_1 = \delta_{-2} - \delta_{-1} = (1, -1, 0, \ldots),$$

$$a_2 = \delta_{+2} - \delta_{-1} = (1, 1, 0, \ldots),$$

$$a_j = \delta_{+j} - \delta_{-1} = (1, 0, \ldots, 1(j\text{th}), \ldots).$$

The unit vectors b_i in momentum space (reciprocal lattice) are determined by

$$b_i \cdot a_j = 2\pi\delta_{i,j}. \tag{2}$$

With the above formulas, the noninteracting Hamiltonian in momentum space is

$$H_0 = \sum_{k,\sigma}\left[\epsilon_f f^\dagger_{k\sigma} f_{k\sigma} + \epsilon_c C^\dagger_{k\sigma} C_{k\sigma} + (V_k C^\dagger_{k\sigma} f_{k\sigma} + \text{H.c.})\right], \tag{3}$$

$$k = \sum_i \frac{k_i b_i}{2\pi}; \quad k_i = \frac{1}{N}, \frac{2}{N}, \frac{3}{N}, \ldots, \tag{4}$$

$$V_k = t^*\left(1 + e^{i(k_1+k_2)} + \sum_{j=1}^{\infty} e^{ik_j} + \sum_{j=3}^{\infty} e^{i(k_1+k_2-k_j)}\right) = t^*\left\{e^{ik_1} + e^{ik_2} + e^{i(k_1+k_2)/2}\left[\left(e^{ik_1+k_2/2} + \sum_{j=3}^{\infty} e^{ik_1+k_2-2k_j/2}\right) + \text{H.c.}\right]\right\}. \tag{5}$$

Here N is the number of unit cells in one axis. Considering k_i as random numbers between 0 and 1, $|V_k|$ obeys Gaussian distribution function,

$$P(|V_k|) = \frac{1}{\sqrt{2\pi t^2}} e^{-|V_k|^2/2t^2}. \tag{6}$$

The exact lattice Green's functions can be expressed as

$$G_{kf}(\omega) = \frac{1}{\omega - \epsilon_f - \Sigma_f(k) - \dfrac{|V_k|^2}{\omega - \epsilon_c}}, \tag{7}$$

$$G_{kc}(\omega) = \frac{1}{\omega - \epsilon_c - \dfrac{|V_k|^2}{\omega - \epsilon_f - \Sigma_f(k)}}, \tag{8}$$

where $\Sigma_f(k)$ is the f electron self-energy resulting from the Coulomb interaction. Within DMFT, $\Sigma_f(k)$ is approximated by the interaction induced self energy Σ_f of the effective SIAM. The Green's function for the corresponding effective SIAM is given by

$$G_{ef}(\omega) = \frac{1}{\omega - \epsilon_f - \Sigma_f - \Delta(\omega)}, \tag{9}$$

where $\Delta(\omega)$ is the hybridization function, which is determined by the self-consistency condition of DMFT. The self-consistency condition states the on-site (local) Green's function for the model should be equal to the Green's function of the effective SIAM,

$$G_{ef}(\omega) = \frac{1}{N}\sum_k G_{fk}(\omega) = \int \frac{P(|V_k|)d|V_k|}{\omega - \epsilon_f - \Sigma_f + i\delta - \dfrac{|V_k|^2}{\omega - \epsilon_c}}. \tag{10}$$

For numerical reasons,[2,23] an extra small imaginary self-energy δ has been added to the f electron Green's function in the above formula for particle-hole asymmetrical cases. This extra self-energy δ can be considered as the self-energy due to impurity scattering. This term turns out to affect the transport properties, as suggested by its physical explanation.

The self-consistent calculations are conducted as follows. For a given self-energy Σ_f, the hybridization function $\Delta(\omega)$ is determined by the self-consistency equation (10). Then NRG (Refs. 19–22) is applied to calculate the spectral functions. The real part of the Green's functions are obtained

from standard Kramers-Kronig transformation. The self-energy Σ_f is determined by the ratio of two Green's functions as[23]

$$\Sigma_f = U\frac{F(\omega)}{G_{ef}(\omega)}, \tag{11}$$

where $F(\omega)=\langle\langle f_\sigma f^\dagger_{-\sigma} f_{-\sigma} | f^\dagger_\sigma\rangle\rangle(\omega)$. The self-consistency condition and self-energy are used to update the hybridization function $\Delta(\omega)$. The above steps are repeated until the self-consistency is achieved.

The current operator is[24]

$$\vec{j} = -it^*\sum_{i,\delta}(\delta f^\dagger_{i+\delta}C_i + \delta C^\dagger_{i+\delta}f_i), \tag{12}$$

where δs are the same as those in the Hamiltonian. The operator can be written in momentum space as

$$\vec{j} = \sum_{x_i}\left[-2t\sum_k \sin(k\cdot x_i)e^{i(k\cdot x_0+\phi)}f^\dagger_k C_k + \text{H.c.}\right]\hat{x}_i, \tag{13}$$

where $x_i=[0,0,\cdots,1(i\text{th}),\cdots]$. $\hat{x}_i$ is the unit vector in x_i direction. x_0 and ϕ are two constants.

The optical conductivity can be expressed as the current-current correlation as[25]

$$d\sigma(\omega) = \frac{1}{i\omega N}\sum_{x_i}\langle\langle j_{x_i}|j_{x_i}\rangle\rangle \tag{14}$$

In the $d\to\infty$ limit, the current operator vertex corrections vanish. The correlation function can be evaluated straightforwardly.[25] The following formula is derived for the optical conductivity,

$$\begin{aligned}\sigma(\omega) = \frac{2\pi}{d}t^2\int dk\int d\epsilon P(|V_k|)A_f(|V_k|,\epsilon)\\ \times\frac{1}{2}\left[A_c(|V_k|,\epsilon+\omega)\frac{n_F(\epsilon)-n_F(\epsilon+\omega)}{\omega}\right.\\ \left.+A_c(k,\epsilon-\omega)\frac{n_F(\epsilon)-n_F(\epsilon-\omega)}{-\omega}\right],\end{aligned} \tag{15}$$

where $A_f(|V_k|,\omega)=-\text{Im}\,G_{kf}(\omega)/\pi$ and $A_c(|V_k|,\omega)=-\text{Im}\,G_{kc}(\omega)/\pi$ are spectral functions. n_F is the Fermi distribution function. $P(|V_k|)$ is defined in Eq. (6). The transport distribution function as defined in the Ref. 26 (also known as generalized relaxation time) can be identified with the above equation to be

$$\tau(\omega) = \frac{2\pi}{d}t^2\int_{-\infty}^{\infty}P(|V_k|)A_f(|V_k|,\omega)A_c(|V_k|,\omega)dk. \tag{16}$$

The Seebeck coefficient can be expressed as the ratio between two linear transport coefficients as[2]

$$L_{11} = \frac{e^2}{\hbar}\int_{-\infty}^{\infty}\left[-\frac{dn_F(\omega)}{d\omega}\right]\tau(\omega)d\omega, \tag{17}$$

$$L_{12} = \frac{e}{\hbar}\int_{-\infty}^{\infty}\left[-\frac{dn_F(\omega)}{d\omega}\right]\omega\tau(\omega)d\omega, \tag{18}$$

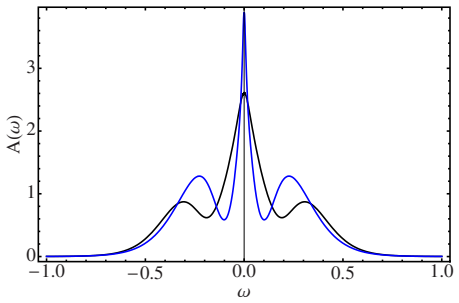

FIG. 2. (Color online) The on-site spectral function for the particle-hole symmetrical case. The black curve is for our model. The blue (gray) curve is for Hubbard model. The parameters are $t=1$ and $U=4$. Unit for ω is $10t$.

$$S = \frac{k_B}{e}\frac{eL_{12}}{k_BT}\frac{1}{L_{11}} = 86\frac{eL_{12}}{k_BT}\frac{1}{L_{11}}(\mu\text{V/K}). \tag{19}$$

The absolute value of Seebeck coefficient can be derived from the above formulas as long as $\tau(\omega)$ is known.

As indicated by the above formulas, transport properties can be discussed only at nonzero temperature. At temperatures much lower than the Kondo temperature T_K, it is reasonable to believe the spectral functions and self energies can be approximated by the corresponding zero-temperature results. The model we consider has a very high Kondo temperature, which can be estimated by[20]

$$k_BT_K = (\Delta(0)U/2)^{1/2}e^{\pi\epsilon_f(\epsilon_f+U)/2\Delta(0)U}. \tag{20}$$

As all terms, including $\Delta(0)$, are of the same order, k_BT_K is roughly of the order $0.1U$. We can calculate the transport coefficients with Kubo formulas for temperature much lower than $0.1U$. Typically, a temperature smaller than $0.01U$ is used for following calculations.

III. RESULTS

The calculation was done for different sets of parameters $(\epsilon_f,\epsilon_c,U)$. The parameters are chosen to satisfy $(\epsilon_f+\text{Re}\,\Sigma_f(0))\epsilon_c>0$. Such a parameter set avoids a gap across the chemical potential in the hybridization function $\Delta(\omega)$. The cases with a gap across the chemical potential in the hybridization function require extra complicated treatments, which is left out of this paper. The results shown below are typical for our calculations.

A. Spectral function

A typical f electron local spectral function for the particle-hole symmetrical case is shown in Fig. 2. $t=1$ and $U=4$ have been chosen for the plot. The local spectral function for Hubbard model with the same parameters is shown for comparison. For the Hubbard model, the one-particle spectrum develops the typical three-peak structure with a quasiparticle peak at $\omega=0$ and the two Hubbard bands at $\pm U/2$. Three-peak structure is also obtained for our model. However, the quasiparticle peak is broadened. The two Hubbard bands shrunk and shifted outward. The Hubbard bands start at $\pm U/2$, instead of having a maximum there. This increases

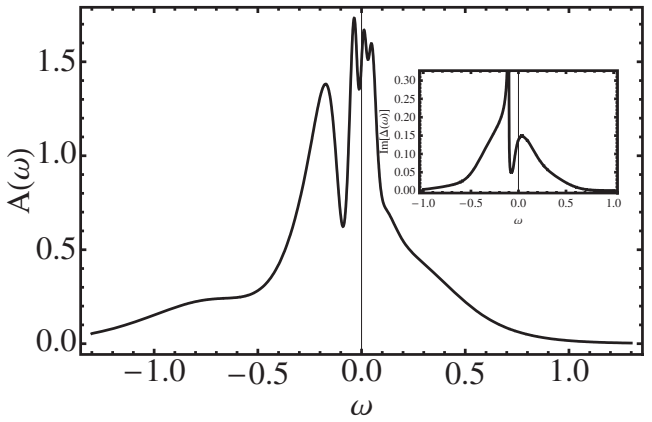

FIG. 3. The on-site spectral function for the particle-hole asymmetrical case. The inset is the imaginary part of hybridization function $\Delta(\omega)$. The parameters are $t=1$, $U=3$, $\epsilon_f=-2.5$, and $\epsilon_c=-0.5$. Unit for ω is $5t$.

the weight of the quasiparticle in our model, which is important for getting better conductivity.

A typical self-consistent f electron local spectral function for the particle-hole asymmetrical case is shown in Fig. 3. $t=1$, $U=3$, $\epsilon_f=-2.5$, and $\epsilon_c=-0.5$ have been chosen for the parameters. The spectral function has a five-peak structure. Three peaks are similar to the peaks of the single-impurity Anderson model or Hubbard model. The negative peak around chemical potential is the quasiparticle peak due to the Kondo effect. Similar to the symmetrical case the Hubbard bands start at band energy ϵ_f, ϵ_f+U, instead of having a maximum there. There are two extra peaks corresponding to the peaks in the hybridization function. The hybridization function is shown in the inset of Fig. 3. The two extra peaks are produced by the peaks of the electron bands. For single-impurity Anderson model, the coupling between the impurity and the band is weak. The structure of the band does not show up in the f electrons spectral function. In our model, the coupling is comparable to the band width and Coulomb interaction. There are two extra peaks due to the structure of the bands.

B. Optical conductivity

The optical conductivity for the symmetrical case is shown in Fig. 4. In the same plot, the optical conductivity for the Hubbard model is shown. The peak at nonzero frequency corresponds to the transition between quasiparticle peak and the Hubbard bands. The positions agree with the peaks in spectral functions. The peaks around the zero frequency are Drude peaks, corresponding to the transitions inside the quasiparticle peaks. The presence of Drude peaks suggest the solutions for the models are metallic. As indicated by the higher Drude peak, the conductivity of our model should be better than that of Hubbard model. This suggests that the inclusion of the linker sites does increase the conductivity of the material. The optical conductivity for an asymmetrical case is shown in Fig. 5. The basic feature is the same as the symmetrical case.

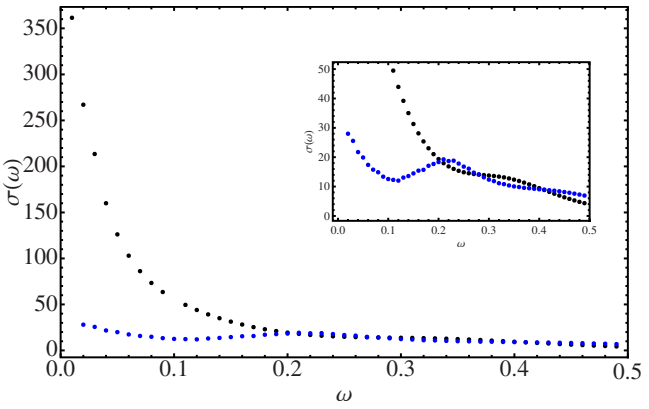

FIG. 4. (Color online) The optical conductivity for the particle-hole symmetrical case. The black dots are for our model. The blue (gray) dots are for the Hubbard model. The parameters are $t=1$ and $U=4$. Unit for ω is $10t$.

The Hubbard model is well known to show a metal-insulator transition with increasing interaction U.[15,23,27] We do not find such transition in our model with particle-hole symmetry. The Drude peaks are always present in the calculation of our model. Based on our calculation and the following theoretical arguments, we believe there is no metal-insulator transition for our model in the symmetrical case. For the symmetrical case, we have

$$\epsilon_c = 0, \tag{21}$$

$$-\epsilon_f - \Sigma_f = c_1\omega + ic_2\omega^2, \tag{22}$$

where c_1 and c_2 are two constants. The second equation results from the exact relation for f electron's self-energy around the chemical potential.[28] The linker's lattice Green's function is reduced to

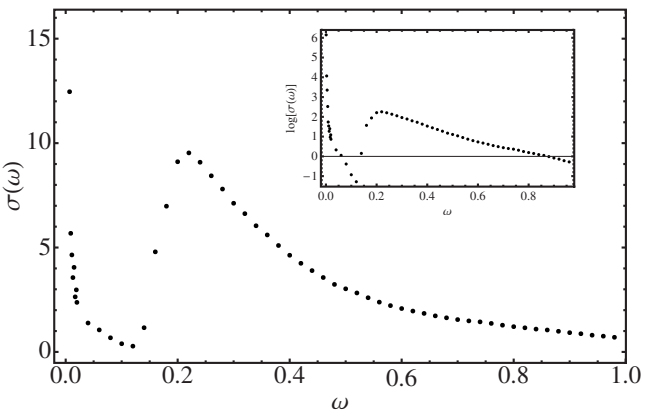

FIG. 5. The optical conductivity for the particle-hole asymmetrical case. The inset shows the same plot with y axis changed to logarithmic scale. The parameters are $t=1$, $U=3$, $\epsilon_f=-2$, and $\epsilon_c=-0.5$. Unit for ω is $5t$.

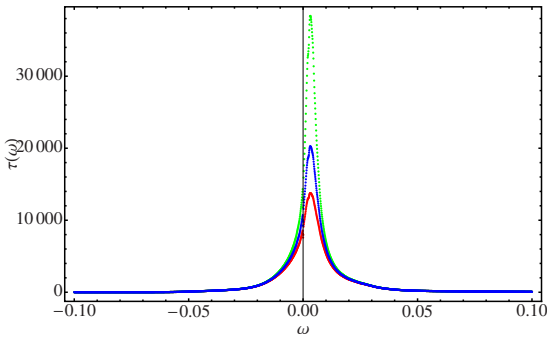

FIG. 6. (Color online) The transport distribution function for the particle-hole asymmetrical case. The $\delta=0.0057U$, $0.0056U$, $0.0055U$ for red, blue, and green plots, respectively. The other parameters are $t=1$, $U=3$, $\epsilon_f=-2.5$, and $\epsilon_c=-0.5$. Unit for ω is $5t$.

$$G_{kc} = \frac{1}{\omega - \dfrac{|V_k|^2}{\omega(1+c_1) + ic_2\omega^2}}. \tag{23}$$

For $|\omega| \ll (1+c_1)/c_2$, the imaginary part of the self-energy can be neglected. It is obvious that the poles near the chemical potential for the linker's lattice Green's function just get normalized by the interaction. These poles form an energy band around chemical potential. Due to the particle-hole symmetry, this band is half filled. According to band theory, this half-filled band is a conducting band. So the model we are considering must always be metallic. If the metal-insulator transition took place, in the insulator phase the f electron's self-energy can be approximated by $-\epsilon_f - \Sigma_f \approx c_1/\omega + i[c_2\omega^2 + \delta(\omega)]$ according to Bulla *et al.*[23] Substituting the above self energy in Eq. (23), we will still get a conducting band with similar arguments. This result contradicts the assumption that the solution is in the insulator phase. This contradiction means that metal-insulator should not take place at all. The above arguments justify the following physical picture: the electron's spectral function in the linker sites is just broaden by coupling to other sites. These linker sites still behave as periodic potential wells for electrons as in the tight-binding model. An extended conduction band should be expected for the model.

C. Seebeck coefficient

The Seebeck coefficient is determined by the transport distribution function $\tau(\omega)$.[26] The Seebeck coefficient is related to the asymmetry of the electron bands.[1] For the symmetrical case, there is no asymmetry in the band. The Seebeck coefficient is zero. For the asymmetrical case, a typical transport distribution function of our model is shown in Fig. 6. As shown in the plot, $\tau(\omega)$ is strongly affected by the extra self-energy δ in Eq. (11). However, different reasonable small δ's produced almost the same f electron spectral functions. This agrees with the physical interpretation of δ as coming from impurity scattering, which just affect the transport properties but not the electron bands. $\tau(\omega)$ of our model always show a single asymmetrical peak near the chemical potential. As proved before by Mahan and Sofo,[26] $\tau(\omega)$ in the shape of Dirac delta function located at $2.4k_BT$ above or below the chemical potential can achieve the best efficiency for the thermoelectric application. Based on that theory and the shape of $\tau(\omega)$ in our model, it is reasonable to believe that high efficiency for thermoelectric applications can be achieved in quantum dot arrays. The best operational temperature is around $\omega_p/2.4k_B$, where ω_p is the position of the peak in $\tau(\omega)$.

The Seebeck coefficient is the ratio between two coefficients with proper units. The absolute value of Seebeck coefficient can be determined. For the example shown in Fig. 6, $\omega_p \approx 0.005$. This model will give the highest figure of merit around the temperature $k_BT=\omega_p/2.4\approx 0.002$ according to above arguments, which is much lower than the Kondo temperature $k_BT_K \approx 0.06$. The Seebeck coefficients calculated at the above temperature are 42, 50, 64, and 106 μV/K, respectively, for $\delta=0.0057U$, $0.0056U$, $0.0055U$, $0.0054U$. Obviously, smaller δ is better for thermoelectric applications. δ should not depend much on the dimension of the model under consideration, as it comes from impurity scattering, which is a local incoherent process. A high Seebeck coefficients with small δ can be achieved in real materials, such as high-quality crystals made of quantum dot arrays with few impurities.[13] The low-temperature maximum Seebeck coefficient for the corresponding Hubbard model (with the same t, ϵ_f, and U) is 51 μV/K, which agrees with previous a study of the Hubbard model.[29] Compared with the Hubbard model, the Seebeck coefficients of our model increases when δ is small.

For a different set of parameters, the Seebeck coefficient tends to increase when $\epsilon_f + \mathrm{Re}\,\Sigma_f(0)$ is closer to the chemical potential. We found the Seebeck coefficient to be as high as 200 μV/K for the parameter set of $t=1$, $U=2$, $\epsilon_f=-1.5$, and $\epsilon_c=-0.5$. As the self-energy δ is used in these calculations, the dependence of the Seebeck coefficient on the parameters are not very conclusive. Further study is necessary to identify the parameter dependence of transport coefficients. However, it is safe to draw the conclusion that the Seebeck coefficients are always quite high for the cases with small ϵ_c and $|\epsilon_c| > |\epsilon_f + \mathrm{Re}\,\Sigma_f(0)|$. These data highlight the potential of quantum dot arrays for thermoelectric applications.

IV. CONCLUSION

Based on above study, it is obvious that the model we studied is quite different from the Hubbard model. This difference is nontrivial. The metal-insulator transition in other strongly correlated models is absent in our model. Probably the phase diagram of our model will also be quite different from the Hubbard model due to different correlations in nearby correlated sites. Our model shows a high Seebeck coefficient and good conductivity, which indicates the possible good thermoelectric properties for arrays of quantum dots.

ACKNOWLEDGMENTS

Numerical renormalization-group calculations were performed using the "Ljubljana NRG" code.

[1] G. D. Mahan, Solid State Phys. **51**, 82 (1997).
[2] C. Grenzebach, F. B. Anders, G. Czycholl, and T. Pruschke, Phys. Rev. B **74**, 195119 (2006).
[3] D. Goldhaber-Gordon, H. Shtrikman, D. Mahalu, D. Abusch-Magder, U. Meirav, and M. A. Kastner, Nature (London) **391**, 156 (1998).
[4] S. M. Cronenwett, T. H. Oosterkamp, and L. P. Kouwenhoven, Science **281**, 540 (1998).
[5] J. Schmid, J. Weis, K. Eberl, and K. v. Klitzing, Phys. Rev. Lett. **84**, 5824 (2000).
[6] T. K. Ng and P. A. Lee, Phys. Rev. Lett. **61**, 1768 (1988).
[7] A. Jerez, P. Vitushinsky, and M. Lavagna, Phys. Rev. Lett. **95**, 127203 (2005).
[8] R. Zitko and J. Bonca, Phys. Rev. B **73**, 035332 (2006).
[9] C. P. Collier, T. Vossmeyer, and J. R. Heath, Annu. Rev. Phys. Chem. **49**, 371 (1998).
[10] G. W. Bryant and W. Jaskolski, Physica E (Amsterdam) **11**, 72 (2001).
[11] F. X. Redl, K. S. Cho, C. B. Murray, and S. O'Brien, Nature (London) **423**, 968 (2003).
[12] J. Cai and G. D. Mahan, Phys. Rev. B **76**, 205116 (2007).
[13] M. Yuan, M. Dirmyer, J. Badding, A. Sen, M. Dahlberg, and P. Schiffer, Inorg. Chem. **46**, 7238 (2007).
[14] G. Sordi, A. Amaricci, and M. J. Rozenberg, Phys. Rev. Lett. **99**, 196403 (2007).
[15] A. Georges, G. Kotliar, W. Krauth, and M. J. Rozenberg, Rev. Mod. Phys. **68**, 13 (1996).
[16] J. Freericks, *Transport in Multilayered Nanostructures* (Imperial College, Singapore, 2006).
[17] K. G. Wilson, Rev. Mod. Phys. **47**, 773 (1975).
[18] W. Hofstetter, Adv. Solid State Phys. **41**, 27 (2001).
[19] H. R. Krishna-murthy, J. W. Wilkins, and K. G. Wilson, Phys. Rev. B **21**, 1003 (1980); H. R. Krishna-murthy, J. W. Wilkins, and K. G. Wilson, *ibid.* **21**, 1044 (1980).
[20] T. A. Costi, A. C. Hewson, and V. Zlatic, J. Phys.: Condens. Matter **6**, 2519 (1994).
[21] K. Chen and C. Jayaprakash, Phys. Rev. B **52**, 14436 (1995).
[22] R. Bulla, T. A. Costi, and D. Vollhardt, Phys. Rev. B **64**, 045103 (2001).
[23] R. Bulla, A. C. Hewson and Th. Pruschke, J. Phys.: Condens. Matter **10**, 8365 (1998).
[24] G. D. Mahan, *Many-Particle Physics*, 3rd ed. (Plenum, New York, 2000).
[25] T. Pruschke, D. L. Cox, and M. Jarrell, Phys. Rev. B **47**, 3553 (1993).
[26] G. D. Mahan and J. O. Sofo, Proc. Natl. Acad. Sci. U.S.A. **93**, 7436 (1996).
[27] X. Y. Zhang, M. J. Rozenberg, and G. Kotliar, Phys. Rev. Lett. **70**, 1666 (1993).
[28] A. C. Hewson, *The Kondo Problem to Heavy Fermions* (Cambridge University Press, New York, 1993).
[29] Th. Pruschke, M. Jarrell, and J. K. Freericks, Adv. Phys. **44**, 187 (1995).